Title

Titanium Disulfide Coated Carbon Nanotube Hybrid Electrodes Enable High Energy Density Symmetric Pseudocapacitors

Journal

Advanced Materials, 30(5)

ISSN

0935-9648

Authors

Zang, Xining
Shen, Caiwei
Kao, Emmeline
et al.

Publication Date

2018-02-01

DOI

10.1002/adma.201704754

Peer reviewed

ADVANCED MATERIALS
www.advmat.de

Titanium Disulfide Coated Carbon Nanotube Hybrid Electrodes Enable High Energy Density Symmetric Pseudocapacitors

*Xining Zang, Caiwei Shen, Emmeline Kao, Roseanne Warren, Ruopeng Zhang, Kwok Siong Teh, Junwen Zhong, Minsong Wei, Buxuan Li, Yao Chu, Mohan Sanghadasa, Adam Schwartzberg, and Liwei Lin**

While electrochemical supercapacitors often show high power density and long operation lifetimes, they are plagued by limited energy density. Pseudocapacitive materials, in contrast, operate by fast surface redox reactions and are shown to enhance energy storage of supercapacitors. Furthermore, several reported systems exhibit high capacitance but restricted electrochemical voltage windows, usually no more than 1 V in aqueous electrolytes. Here, it is demonstrated that vertically aligned carbon nanotubes (VACNTs) with uniformly coated, pseudocapacitive titanium disulfide (TiS_2) composite electrodes can extend the stable working range to over 3 V to achieve a high capacitance of 195 F g^{-1} in an Li-rich electrolyte. A symmetric cell demonstrates an energy density of 60.9 Wh kg^{-1}—the highest among symmetric pseudocapacitors using metal oxides, conducting polymers, 2D transition metal carbides (MXene), and other transition metal dichalcogenides. Nanostructures prepared by an atomic layer deposition/sulfurization process facilitate ion transportation and surface reactions to result in a high power density of 1250 W kg^{-1} with stable operation over 10 000 cycles. A flexible solid-state supercapacitor prepared by transferring the TiS_2–VACNT composite film onto Kapton tape is demonstrated to power a 2.2 V light emitting diode (LED) for 1 min.

Transition metal dichalcogenide (TMDC) materials, such as MoS_2, WS_2, and $MoSe_2$, have been widely studied in electrochemical applications as sensors,[1] catalysts,[2] and energy storage materials.[1,3] Among all TMDCs, TiS_2 is the lightest and cheapest[4] with the following potential benefits for lithium-based energy storage systems: (1) highest energy density storage capability among TMDCs,[4] (2) fast ion transportation rate,[5] (3) low volume expansion during reversible charge–discharge cycles,[6] and (4) no phase change during lithium ion intercalation.[4] However, TiS_2 suffers from mechanical degradation during ionization and deionization and has less desirable electrical conductivity.[7] Conformal coating of TiS_2 onto highly conductive 3D porous networks such as vertically aligned carbon nanotubes (VACNTs) improves electrical conductivity, increases surface areas, and helps the mechanical stability in electrochemical reactions.[8,9] Potential methods include chemical vapor deposition (CVD),[10] electro- and electroless plating,[11] and atomic layer deposition (ALD).[12] Both CVD- and plating-based processes encounter challenges in uniform coverage and crystallinity while the ALD deposition can achieve uniform and conformal coverage on porous, high-aspect-ratio structures such as VACNTs.[13] Not only does conventional ALD of TiS_2 use $TiCl_4$ and highly toxic H_2S as precursors, the subsequent production of sulfur contaminates ALD chambers.[12] In contrast, here we developed a two-step process that combines ALD of TiN[14] with a following CVD

Dr. X. Zang, C. Shen, E. Kao, Dr. J. Zhong, Dr. M. Wei, Prof. L. Lin
Berkeley Sensor and Actuator Center
Berkeley, CA 94704, USA
E-mail: lwlin@berkeley.edu
Dr. X. Zang, C. Shen, E. Kao, Dr. J. Zhong, Dr. M. Wei, B. Li, Y. Chu, Prof. L. Lin
Mechanical Engineering
University of California Berkley
Berkeley, CA 94704, USA
Prof. R. Warren
Mechanical Engineering
University of Utah
Salt Lake City, UT 84112, USA
R. Zhang
National Center for Electron Microscopy
Lawrence Berkeley National Lab
Berkeley, CA 94720, USA
Prof. K. S. Teh
School of Engineering
San Francisco State University
San Francisco, CA 94132, USA
Dr. M. Sanghadasa
U.S. Army RDECOM AMRDEC
Redstone Arsenal
AL 35898, USA
Dr. A. Schwartzberg
Molecular Foundry
Lawrence Berkeley National Lab
Berkeley, CA 94720, USA

DOI: 10.1002/adma.201704754

sulfurization to fabricate TiS_2 composite-coated VACNT electrodes with desired nanostructures. Such ALD/sulfurization process could further be expanded to construct uniform coaxial coatings of chalcogenide (MoS_2, WS_2, etc.) onto high-aspect-ratio templates. Further characterizations demonstrate that the pseudocapacitive electrodes show a capacitance of 195 F g^{-1} within a potential range of 3 V in a lithium-rich aqueous electrolyte, corresponding to an energy density of 60.9 Wh kg^{-1} for a symmetric cell, which is exceptional among reported symmetric pseudocapacitors.

The structure of the TiS_2-coated VACNT hybrid electrodes is illustrated in **Figure 1**a, in which a TiN layer is deposited by ALD and sulfurized to be TiS_2 composite via annealing in sulfur powder at relatively low temperature (300 °C), maintaining conformal coating on VACNTs during the entire process. Such electrodes show high electrochemical capacitance due to the intercalation of Li ions with TiS_2 composite. Furthermore, the electrode material successfully operates within a large potential window of 3 V in a lithium-rich "water-in-salt" electrolyte that has only been applied in battery.[15,16] As such, the energy density of the supercapacitor cell, proportional to the capacitance multiplied by voltage squared, outperforms most state-of-the-art symmetric pseudocapacitors using metal oxides, metal chalcogenides, and metal carbides[17–24] with comparable results to Li-ion batteries (Figure 1b). TiS_2–VACNT composites in ultrahigh-concentration LiTFSI electrolyte represents a specific energy 900 times that of bare VACNTs using a 0.5 M H_2SO_4 electrolyte. Furthermore, when compared to other electrodes of similar structures made of VACNT forests coated with pseudocapacitive materials, such as RuO_x,[13] TiN,[14] and MoS_2,[18] TiS_2–VACNTs show superior capacitance, energy density, and power density. Moreover, TiS_2 composite coated on carbon nanotube (CNT) inherits the low phase transformation rate in lithiation and delithiation cycles[4] while maintaining a low deformation ratio (<5%) and high capacitance retention (≈95%) after 10 000 cycles of cyclic voltammetry testing (Figure 1c). The CNT forest network helps immobilize the TiS_2 coating layer to release the stress and deformation in the charging–discharging cycles to improve the mechanical stability of TiS_2 for high cycle operations.[7]

The conductive, porous VACNT forest is grown on a silicon or stainless steel substrate[8] and the diameter of an as-grown CNT is 13 ± 5 nm (Figure S1, Supporting Information). Afterward, 500 cycles of ALD TiN are deposited for a uniform and conformal coating of TiN with a final TiN/CNT diameter of 130 ± 15 nm (Figure S2, Supporting Information). Deposition rate varies from 0.06 to 0.25 nm per cycle depending on temperature and cycle numbers; the average growth rate for 500 cycles is ≈0.11 and ≈0.12 nm per cycle for 800 cycles (Figure S2, Supporting Information).[25,26] Under sulfur vapor annealing at 300 °C for 30 min, the amorphous TiN layer is converted to polycrystalline TiS_2 composite (**Figure 2**a) and maintains conformal coating on CNTs (Figure 2b). High-resolution transmission electron microscopy (Figure 2c) reveals that the resulting

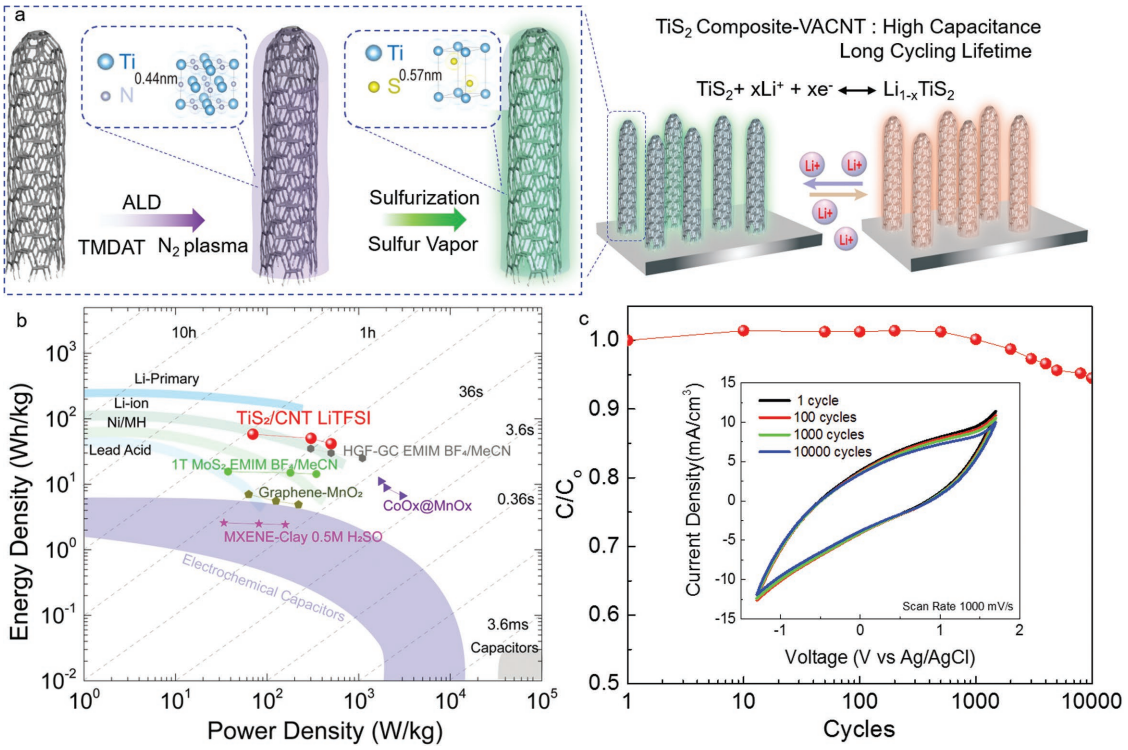

Figure 1. TiS_2–VACNT hybrid fabrication process and advantage as pseudocapacitor electrodes. a) TiS_2–VACNT composite electrodes synthesized by a two-step process: TiN is coated onto VACNT by atomic layer deposition and converted to TiS_2 composite in a sulfur vapor environment. The high capacitance energy storage in Li^+ electrolyte is achieved by electron-double-layer and TiS_2 composite–Li intercalation. b) Ragone plot for state-of-the-art energy storage systems showing TiS_2–VACNT composite with the highest energy density among various families of noncarbon materials, including metal oxides, metal chalcogenides, and metal-carbide-based system.[17–24] c) Long-term cyclability of the TiS_2–VACNT composite electrode in the 21 m LiTFSI electrolyte.

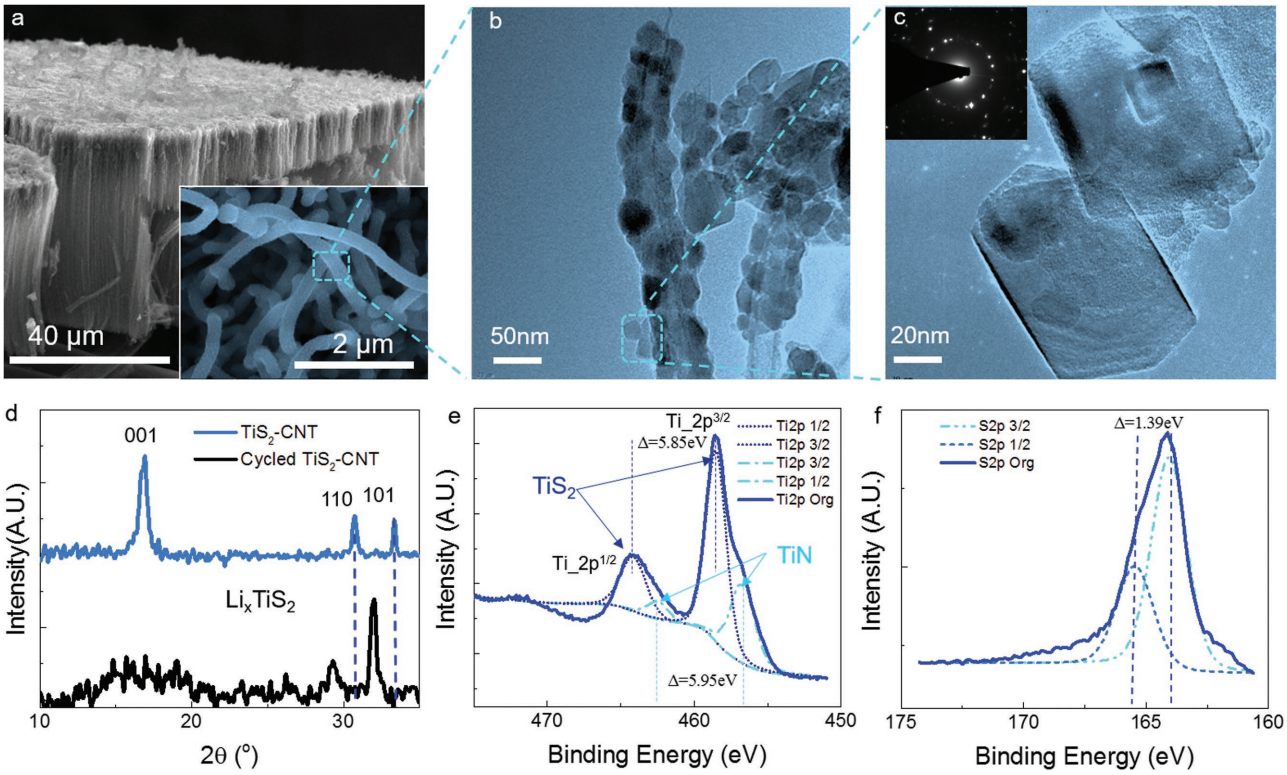

Figure 2. Material characterization of the TiS_2–VACNT composite electrodes. a) SEM image after a 500-cycle ALD TiN deposition process followed up with a sulfurization step; inset: magnified SEM image showing individual electrodes with a diameter of 210 ± 13 nm. b) TEM image of CNT coated with sulfurized TiS_2 composite particles. c) Zoomed-in TEM image of hexagonal TiS_2 composite nanoparticles in (b). d) XRD showing the (001) peak at 16.6°, (110) at 30.4°, and (101) at 33.1°. The (001) peak is broadened while the other two peaks shift to slightly smaller angles after intercalation in LiTFSI. e) XPS spectrum for TiS_2 composite–VACNT, in which split Ti_2p$^{1/2}$ and Ti_2p$^{3/2}$ peaks indicate different composition of TiS_2 and TiN. f) XPS spectrum of sulfur peak of TiS_2 composite, with S_2p$^{1/2}$ and S_2p$^{3/2}$ split peaks.

materials are hexagonal-shaped structures with characteristic polycrystalline diffraction rings, in-plane 0.3 nm lattice distance, and (001) zone axis of the CdI_2-type symmetry. X-ray diffraction (XRD) shows standard peaks of TiS_2 composite with the low angle at 16.6° due to the (001) stacking structures, and the (110) and (101) peaks by using a Co X-ray diffraction source (Figure 2d). XRD of cycled TiS_2 electrodes is also shown in Figure 2d for comparison. Split Ti_2p peaks indicate composite Ti^{4+} and Ti^{3+} (residual TiN) with different spin–orbit splitting showing different energy difference (Figure 2e). Figure 2f reveals S_2p$^{1/2}$ and S_2p$^{3/2}$ spin splitting with energy different of 1.39 eV. Sulfur peaks of S_2s at the binding energy of 228.8 eV and S_2p at the binding energy of 164.8 eV are observed after one and three times of repeated sulfur annealing while the relative distance and intensity of the peaks are almost the same (Figure S3, Supporting Information), implying that additional sulfurization does not contribute to further material conversions from TiN to TiS_2 composite.

In **Figure 3**a, cyclic voltammetry (CV) results show that TiS_2 composite–VACNT in 21 m (mol kg^{-1}) LiTFSI electrolyte exhibits over ≈100 times the specific capacitance (per projected surface area) of as-grown VACNT electrode in 0.5 M H_2SO_4 electrolyte. Two key mechanisms are believed to assist this significant increase: (1) intercalation of Li–S into and out of the TiS_2 composite and (2) the increase of working voltage window from 1 to 3 V. It is found that the specific capacitance increases ≈4 times from the VACNT–H_2SO_4 system to the VACNT–LiTFSI system and 26.8 times from the VACNT–LiTFSI system to the TiS_2 composite–VACNT–LiTFSI system; the total increase is more than 100 times higher capacitance. Furthermore, the length of VACNT is found to slightly affect the performance of the TiS_2 composite–VACNT electrode systems (Figure 3b; Figure S4, Supporting Information). The system made of 4 μm thick VACNT grown on stainless steel has about 15% higher specific capacitance (195 F g^{-1}) as compared with that of the system made of 40 μm thick VACNT grown on silicon (168 F g^{-1}), as shown in Figure S4 (Supporting Information). Systems made of shorter VACNT electrodes could benefit from increased sulfur diffusion in the annealing process for the conversion of TiS_2 composite and smoother ion diffusion during the charge–discharge process. In the fitted capacity versus reverse of the square root of scan rate in Figure 3c, the larger constant of $\nu^{1/2}$ than the interception constant indicates a near 2:1 ratio of diffusive to capacitive behavior in the cyclic voltammetry curve, consistent with the nature of Li^+–Ti–S intercalation. It is also noted that even with over 60% diffusive capacitance, there is no obvious lithiation peak, which we could attribute to the limited, nanoscale TiS_2 depth and high surface area of VACNT forest that lead to more surface reactions at relatively high scan rates as compared to battery discharge rate. Similarly, if the 10 m LiCl electrolyte is used as the electrolyte (Figure S5, Supporting Information),

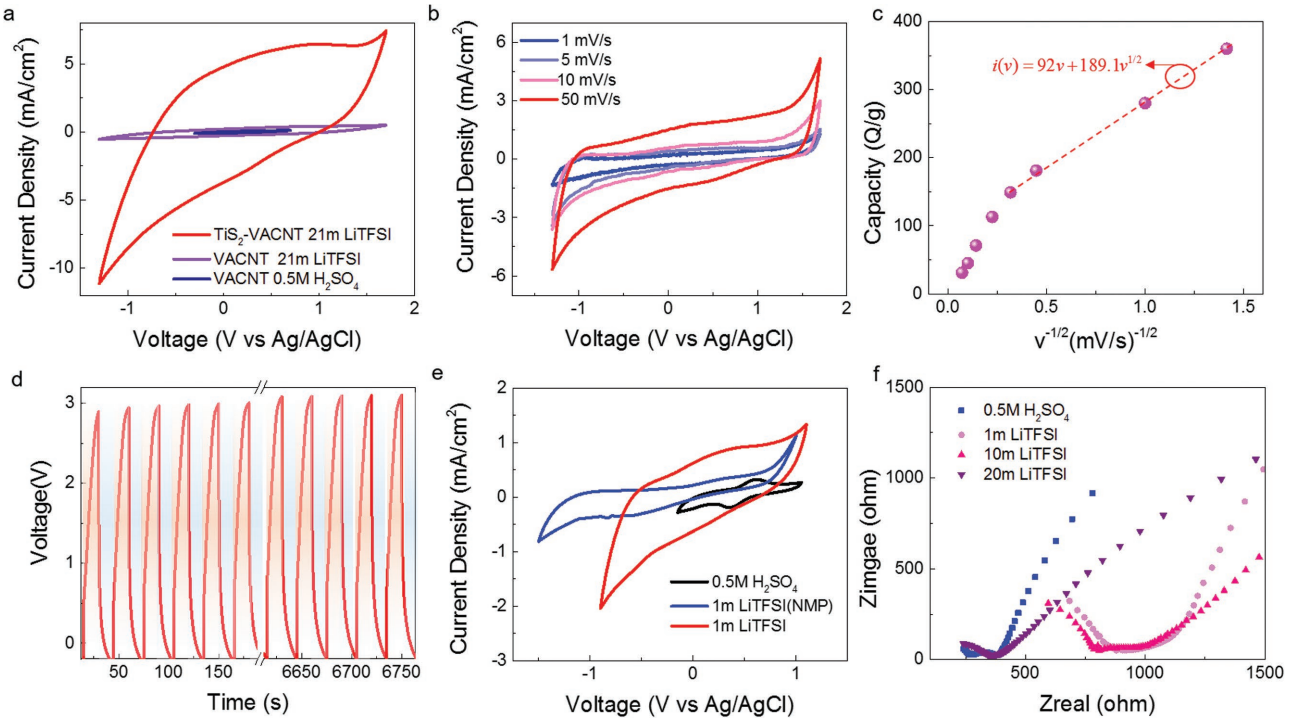

Figure 3. Electrochemical testing results of TiS_2–VACNT composite electrodes in the 21 m LiTFSI electrolyte. a) CV results from three systems: as-grown VACNT electrodes in 0.5 M H_2SO_4 electrolyte, in 21 m LiTFSI electrolyte, and TiS_2–VACNT composite electrodes in 21 m LiTFSI electrolyte. b) CV results of TiS_2–VACNT composite electrode in 21 m LiTFSI electrolyte under different scanning rates from 1 to 50 mV s^{-1}. c) Analysis of the energy storage capacity versus $v^{-1/2}$. d) Repeating chronopotentiometry charge–discharge tests of TiS_2 composite/CNT in 21 m LiTFSI with a discharging current density of 300 μA cm^{-2}. e,f) CV and Nyquist plots of TiS_2–VACNT composite electrodes in multiple electrolytes.

no lithiation peaks are observed at 10 mV s^{-1} with only a small peak at 2 mV s^{-1}. Due to such observations, as well as two other facts including no plateaus shown in the chronopotentiometry charge–discharge tests (Figure 3d) and stable operation in symmetric two-electrode cells, we consider our composite electrodes as pseudocapacitive instead of battery like.

It is estimated that the density of the TiS_2–VACNT composite electrodes is 0.9 g cm^{-3} (Supporting Information) and the volumetric specific capacitance up to ≈216 F cm^{-3} (Figure S4, Supporting Information), such that chronopotentiometry current density of 1 mA cm^{-2} is equivalent to 1.11 A g^{-1} (Figure S6a, Supporting Information). A low Coulombic efficiency has been observed in the test, which can be caused by two possible reasons. One is the slow chemical kinetics of Li^+ intercalations in chalcogenide materials. The other is the self-discharging of the device caused by the leakages through Ohmic resistance and side reactions, which exist in all electrochemical energy storage devices. Nevertheless, the specific capacitance of electrodes tested between −1–0.8 V results in similar values and kinetics under different voltage scanning rates. Although the high capacitance is demonstrated with the 3 V working window (Figure S6b,c, Supporting Information), high voltage operations could induce aging for electrodes and electrolyte such that a slightly smaller working window such as 2.7 V is recommended for longer lifetime. When a 1.5 mA cm^{-2} current density source is used, it takes about 15 s to charge–discharge the system to 3 V (Figure 3d). It is found that the TiS_2–VACNT composite network helps to mechanically stabilize the system during the cycling tests: >95% of original capacitance is maintained after 10 000 operation cycles (Figure 1c). Results show that the capacitance increases slightly during the initial cycles and drops in the last few thousands of cycles. We think that the slight increase of the capacitance in the initial cycling process is caused by two possible mechanisms: (1) the ion insertion and dissociation processes improve the conductivity and (2) the surface wettability improves. On the other hand, the reason for performance decay is likely the decreased lithiation depth. From the X-ray photoelectron spectroscopy (XPS) and XRD results, we see ions in LiTFSI gradually diffuse or intercalate into the lattice after cycling. Even though there is no solid electrolyte interface formed, the deformed surface layer could possibly block the further ion transportation.

There is also no obvious change in the morphology of the electrodes (Figure S7, Supporting Information). The TiS_2 shows limited lattice expansion after cycling (Figure 2d), The (001) peak is broadened and shifted, while the (110) and (101) peaks shifted from 30.4° to 29.4° and 33.1° to 31.9°, respectively, indicating lattice deformation of 3.1% and 4.5%, respectively. Meanwhile XPS spectrum of cycled TiS_2 implies residual Li^+ in the lattice indicated by the slight Ti_2p shift and electrolyte absorption with S_2p side peak presented (Figure S8 and Table S1, Supporting Information). Furthermore, the system made of an 800-cycle ALD TiN does not show obvious improvement of specific capacitance as compared with the system made of 500-cycle ALD TiN; longer sulfurization annealing does not significantly improve performance (Figure S9, Supporting Information).

Table 1. TiS_2 composite–VACNT electrodes in different electrolytes (NMP: *N*-methyl-2-pyrrolidone).

V vs Ag/AgCl	Min. potential [V]	Max. potential [V]	Potential window [V]	Capacitance F g^{-1} [10 mV s^{-1}]
0.5 M H_2SO_4	−0.2	1.0	1.2	10.4
1 m NaCl	−0.4	0.1	0.5	0.2
1 m LiCl	−0.4	1.0	1.4	18.75
10 m LiCl	−0.5	1	1.5	30
20 m LiCl	−1.3	1.05	2.35	80
1 m LiTFSI	−0.8	1.1	1.9	86
10 m LiTFSI	−1	1.2	2.3	102
21 m LiTFSI	−1.3	1.7	3	120
1 m LiTFSI in NMP	−1.5	0.9	2.4	31.25

Effects of different electrolytes, 0.5 M H_2SO_4, 1 m LiTFSI in *N*-methyl-2-pyrrolidone (NMP), and 1 m LiTFSI (Figure 3e), were observed under different operation voltage windows and organic NMP-based electrolyte presented slightly higher working windows. However, the TiS_2–VACNT composite electrode system in 1 m LiTFSI electrolyte dissolved in NMP can produce only about one-third of specific capacitance than that of the same electrode system in 1 m LiTFSI electrolyte dissolved in distilled (DI) water (**Table 1**; Figure S10, Supporting Information) due to the lower ionic activity in organic solvent.[27] Other key results from the Li^+-rich electrolytes are summarized in Table 1. Working voltage window was found to scale with Li^+ concentration as the activity of water molecule is suppressed by the high concentration of cathodic Li^+ and anodic $TFSI^-$ or Cl^- (additional results are provided in Figure S11 in the Supporting Information). As a result, the hydrogen evolution reaction (HER) and oxygen evolution reaction (OER) depopulate to broaden the stable operation voltage window.[16] Specifically, high concentrations of LiTFSI extend the electrochemical window from 1.9 V (1 m) to 3 V (21 m), and high concentrations of LiCl extend the window from 1.4 V (1 m) to 2.35 V (20 m). Furthermore, the large TFSI anion forms higher Helmholtz layer potentials to increase the threshold of oxygen evolution swing to 1.7 V (Cl^- solution occurs at 1.05 V). On the other hand, electrolytes based on H_2SO_4 and NaCl (H^+ or Na^+ ions) do not exhibit intercalation with TiS_2 composite. In fact, H^+ increases the probability of hydrogen evolution by lowering overpotential in the hydrogen evolution reaction, decreasing the electrochemical voltage window. Furthermore, high LiTFSI concentration increases the conductivity of ions and lowers electrolytic impedence[28] (Figure 3f). These characteristics in high-concentration LiTFSI solution work to improve both energy density and power density of Li-ion-based storage systems.

The electrochemical voltage window is further determined by the coated active material (VACNT works as an inert electrode). Experimentally, stable ranges of −1.3 to 1.7 V versus Ag/AgCl (1.9–4.9 V vs Li/Li^+) for the TiS_2–VACNT composite electrodes under the 21 m LiTFSI electrolyte are observed (**Figure 4**a), higher than the other three tested pseudocapacitive materials, RuO_x, MoS_2, and TiN. Both RuO_x–VACNT and MoS_2–VACNT electrode systems act as HER/OER catalysts and decrease the stable operation voltage window.[29,30] The TiN–VACNT electrode system shows an undesirable broad electrochemical peak near −0.4 V which could be attributed to either hydrolysis or TiN–TiO_2 impurity transition reactions due to the instability of TiN in acidic media.[31] As such, the TiS_2–VACNT composite electrode system provides unique characteristics in the 21 m LiTFSI: (1) a large stable electrochemical operation voltage window, (2) high specific capacitance, (3) high power density, and (4) high energy density as compared with the other electrode systems. Specifically, experimental results show that the TiS_2–VACNT composite system can result in the largest enclosed area in the CV tests than those of tested RuO_x–, MoS_2–, and TiN–VACNT systems with a scanning rate of 100 mV s^{-1} (Figure 4b), and has the highest capacitance density under various scan rates (Figure 4c). In Figure 4c, specific capacitance at 10 mV s^{-1} maintains 120 F g^{-1} which corresponds to charging 12 C g^{-1} within 5 min. Such high charging rate is difficult to achieve in a battery system. Although RuO_x is considered one of the highest capacitance materials,[32] it is incapable of effective Li^+ intercalation in Li-rich electrolytes. MoS_2 has a higher density (5.06 g cm^{-3}) than that of TiS_2 composite (supplementary materials) which leads to unfavorable gravimetric capacitance and energy density. In this work, MoS_2–VACNT electrodes are also shown to suffer from poor coverage onto the individual CNT electrodes as most of the deposition forms a layer on the top of the VACNT structure (Figure S12, Supporting Information). TiN shows good electrical conductivity but its electrochemical performance is not comparable with TiS_2 composite in Li^+ or non-Li^+ electrolytes. Figure 4d summarizes the nominal energy density and working potential window for the tested electrodes presented in this paper. Figure 4e shows the measured energy density and power density of all tested electrodes under different scan rates to show high energy density and high power density of the different electrodes. Figure 4f records the relationships between capacitance density, energy density, and power density for all tested electrodes.

In this paper, we attribute the exceptional energy density of TiS_2–VACNT hybrid systems to the large working voltage window and intercalation-induced capacitance. Although some oxide materials (such as RuO_x and MnO_x) also provide high capacitance, smaller operation voltage windows in conventional acidic and basic electrolytes limit their energy density (Table S2, Supporting Information). Using conventional organic solvent may promotes cell voltage by eliminating hydrolysis but low ionic conductivity and diffusion coefficient degrade the performance.[33] Since the aqueous electrolyte can easily be made in ambient conditions to eliminate possible safety issues, the TiS_2–VACNT composite electrode system with 21 m LiTFSI electrode is preferable to conventional Li^+-rich solutions for various systems.

As a practical demonstration, a full symmetric cell device is constructed using a two-electrode design on filter paper (Fisher Scientific, P5 grade) and tested under a broad range of scan

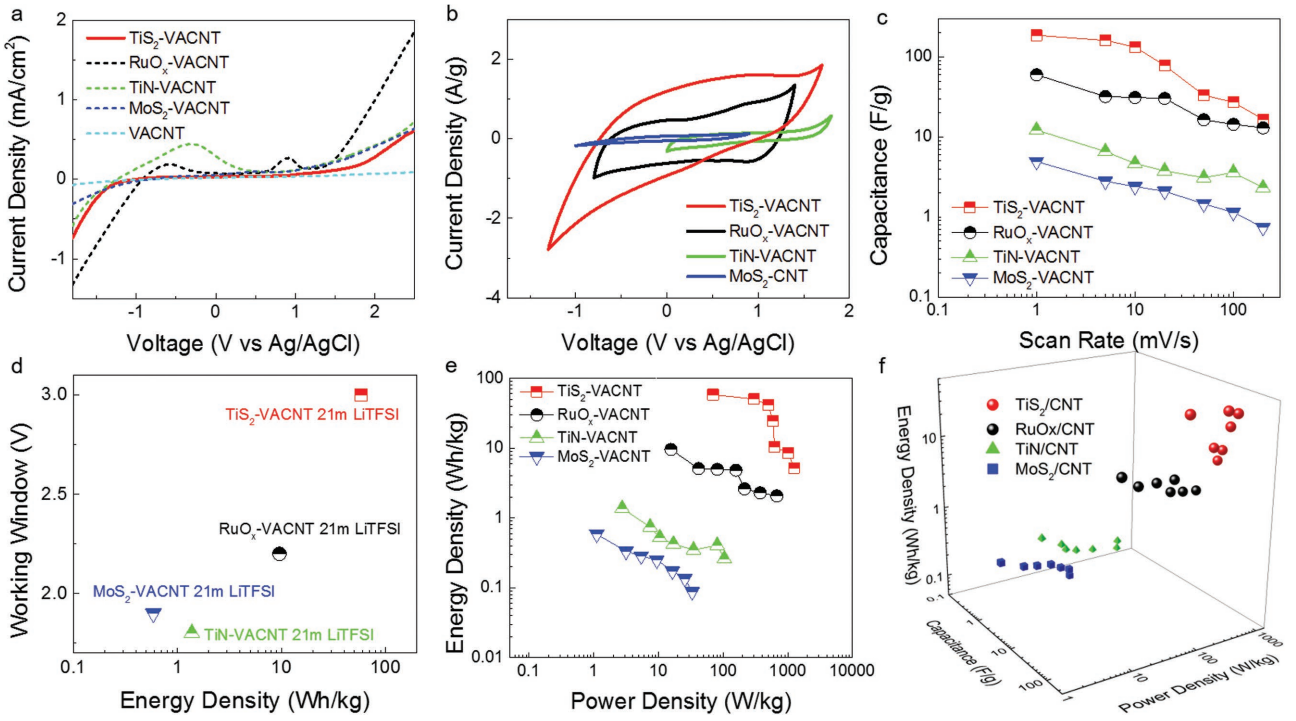

Figure 4. TiS_2–VACNT composite electrodes outperform other VACNT-based electrodes coated with high-energy pseduocapacitive materials such as RuO_x, TiN, and MoS_2. a) Linear sweep voltammetry (LSV) results of as-grown VACNT, TiS_2 composite–, RuO_x–, TiN–, and MoS_2–VACNT electrodes in 21 m LiTFSI electrolyte under a scan rate of 5 mV s^{-1}. Both TiS_2 composite–VACNT and pristine VACNT electrodes exhibit a 3 V stable operation window, while other electrodes have either broad redox peaks or hydrolysis reactions at a low voltage to reduce the electrochemical operation window. b) CV results of four different electrodes in 21 m LiTFSI electrolyte under a scan rate of 100 mV s^{-1}. c) Capacitance density versus scan rate of the four-electrode systems. d) Operation voltage window versus energy density for the four-electrode systems. e) Measured energy density versus power energy density of the four-electrode systems. f) Measurement results and comparison of the energy density, power density, and capacitance of the four VACNT electrodes coated with different materials.

rates from 2 to 100 mV s^{-1} (**Figure 5**a). The Nyquist plot shows the internal resistance to be about 1000 Ω, consistent with single cell impedance testing result of 400 Ω (Figure 5b). By transferring two TiS_2–VACNT composite film structures onto Kapton tape with filter paper as the separator, a flexible, fully operational cell is built. The semisolid 21 m LiTFSI/5% PVA electrolyte is applied to measure a capacitance of 60 mF cm^{-2} at a scan rate of 15 mV s^{-1}. This device is able to power a 2.2 V LED for 1 min (Figure 5c). In the future, large-scale TiS_2–VACNT can be transferred and patterned onto versatile substrates with better elastic properties and structural designs in order to make flexible and stretchable energy storage devices with high energy densities.[34,35]

Three factors allow for exceptionally high energy density (reaching a maximum of 60.9 Wh kg^{-1} and 54.8 mWh cm^{-3}) for TiS_2–VACNT composite electrodes: (1) large electrochemical voltage window of 3 V due to the chemical stability of TiS_2 composite in ultrahigh concentration, 21 m LiTFSI electrolyte;

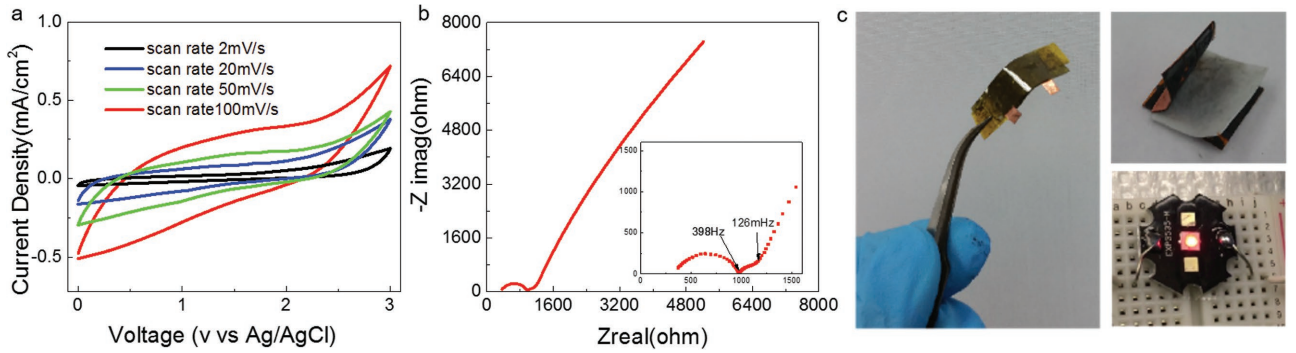

Figure 5. Demonstration for potential practical applications. a) CV of a symmetric full cell made of a two-electrode design with a filter paper as the separator in between with the 21 m LiTFST electrolyte. b) Impedance measurement results. c) A flexible fully cell energy storage system is built by transferring two TiS_2–VACNT film structures onto a Kapton tap with a filter paper in between as the separator with the LiTFSI/PVA/H_2O electrolyte to power up a 2.2 V LED for 60 s.

(2) effective intercalation of Li^+ into TiS_2–VACNT composite for high gravimetric capacitance of 195 F g^{-1}; and (3) nanocrystallinity of TiS_2 composite and ultrahigh surface area of VACNT framework promote surface reactions instead of bulk behavior for a maximum power density of 1250 W kg^{-1} (≈1.13 W cm^{-3}) and cycleability of more than 10 000 charge–discharge cycles with >95% capacitance retention. TiS_2–VACNT composite electrodes are compared with prepared RuO_x–, MoS_2–, TiN–VACNT and bare VACNT electrode systems and compared with other published works of various high-performance oxide, chalcogenide, and MXene energy storage systems. The TiS_2–VACNT composite electrode system in 21 m LiTFSI electrolyte achieves the highest maximum energy density among these supercapacitors. Furthermore, by decreasing the thickness of TiS_2 composite while increasing surface area of the highly porous VACNT network, we are able to achieve high power density. As a result, the large volumetric deformation during the charge–discharge operations is prevented to preserve the long-term stability of TiS_2 composite. So far, only a few graphene/activated graphene with extremely high surface areas report slightly higher energy densities in organic electrolyte or ionic liquid.[36,37] With further efforts to modify the composition of TiS_2 composite and decrease the impurities/defects, the performance of hybrid TiS_2 composite–VACNT LiTFSI systems could be further enhanced. Other aspects of such supercapacitors materials will be studied, including volumetric and areal capacitance[38] for potential applications with specific requirement.

Experimental Section

Synthesis of TiS_2–VACNT Composite Electrodes: A thermally grown silica layer on silicon serves as the basis of the VACNT substrate. A 50/10/5 nm Mo/Al/Fe thin film is evaporated as the catalyst layer and VACNTs are grown by CVD in a carbon-rich environment. The height (thickness) of the VACNT forest is controlled by processing time.[8] Alternatively, the VACNT electrodes are synthesized on a stainless-steel substrate with a passivation layer of atomic layer deposited Al_2O_3 (Cambridge Fiji F200 Plasma ALD). The same ALD tool is used to coat TiN onto the VACNT framework, with TDMAT (0.05 s) and N_2 plasma (5 s, 300 W) as precursors and 5 s argon purge at 300 °C. The TiN–VACNT forest is annealed in sulfur vapor at 150, 250, 300, or 350 °C in a furnace (Lindbergh Thermal) for 30 min.

Synthesis of RuO_x–VACNT Electrodes: RuO_x is deposited onto the VACNT electrodes using ALD with bis(ethylcyclopentadienyl) ruthenium(II) ($Ru(EtCp)_2$) and oxygen (O_2) as precursors. Pulse times for $Ru(EtCp)_2$ and O_2 are 1 s and 10 s, respectively, with 5 s argon gas purge. During the ALD process, substrates were heated to temperatures ranging from 270 to 400 °C.[13]

Synthesis of MoS_2–VACNT Electrodes: MoS_2 is grown by a second CVD process, using stoichiometric sulfur and MoO_3 as precursors and 300 sccm of Ar as the carrier gas. The holders for sulfur, MoO_3, and CNT are separated in different locations and heated to 400, 650, and 650 °C, respectively.

Materials Characterization: Scanning electron microscopy (SEM, FEI Quanta 3D), transmission electron microscopy (TEM, FEI Tecnai) are employed to study the morphology and structure of as-grown VACNT, TiN–VACNT, and TiS_2 composite–VACNT. X-ray diffraction (Bruker D8) is performed to study the crystallinity and X-ray photoelectron spectroscopy (CHI) is used to study the surface element components of samples. Cycled TiS_2–VACNT samples are washed by DI water and vacuum dried before XRD and XPS tests.

Electrochemical Testing: Ag/AgCl is used as the reference electrode to study VACNT, TiN–, TiS_2 composite–, RuO_x and MoS_2–VACNT electrode systems for comparisons in different electrolytes. Linear sweep voltammetry, cyclic voltammetry, chronopotentiometry, and EIS impedance tests are performed by an electrochemistry workstation (Gamry Ref 600) with different modules.

Supporting Information

Supporting Information is available from the Wiley Online Library or from the author.

Acknowledgements

This work was performed in part at the Molecular Foundry, a User Facility supported by the Office of Science, Office of Basic Energy Sciences, of the U.S. Department of Energy under Contract No. DE-AC02-05CH11231 and supported in part by Berkeley Sensor and Actuator Center, an NSF/Industry/University Research Collaboration Center.

Conflict of Interest

The authors declare no conflict of interest.

Keywords

atomic layer deposition (ALD), high energy density storage, titanium sulfides, transition metal dichalcogenides (TMDC), vertically aligned carbon nanotubes (VACNTs)

Received: August 21, 2017
Revised: October 20, 2017
Published online: December 11, 2017

[1] M. Pumera, A. H. Loo, *TrAC, Trends Anal. Chem.* **2014**, *61*, 49.
[2] J. Zhang, S. H. Liu, H. W. Liang, R. H. Dong, X. L. Feng, *Adv. Mater.* **2015**, *27*, 7426.
[3] S. Y. Chen, C. X. Zheng, M. S. Fuhrer, J. Yan, *Nano Lett.* **2015**, *15*, 2526.
[4] G. A. Muller, J. B. Cook, H. S. Kim, S. H. Tolbert, B. Dunn, *Nano Lett.* **2015**, *15*, 1911.
[5] Z. W. Seh, J. H. Yu, W. Y. Li, P. C. Hsu, H. T. Wang, Y. M. Sun, H. B. Yao, Q. F. Zhang, Y. Cui, *Nat. Commun.* **2014**, *5*, 5017.
[6] E. A. Suslov, O. V. Bushkova, E. A. Sherstobitova, O. G. Reznitskikh, A. N. Titov, *Ionics* **2016**, *22*, 503.
[7] E. J. Frazer, S. Phang, *J. Power Sources* **1981**, *6*, 307.
[8] Y. Q. Jiang, P. B. Wang, X. N. Zang, Y. Yang, A. Kozinda, L. W. Lin, *Nano Lett.* **2013**, *13*, 3524.
[9] S. W. Lee, J. Kim, S. Chen, P. T. Hammond, Y. Shao-Horn, *ACS Nano* **2010**, *4*, 3889.
[10] M. S. Whittingham, J. A. Panella, *Mater. Res. Bull.* **1981**, *16*, 37.
[11] J. Chen, S. L. Li, Z. L. Tao, F. Gao, *Chem. Commun.* **2003**, *8*, 980.
[12] V. Pore, M. Ritala, M. Leskela, *Chem. Vap. Deposition* **2007**, *13*, 163.
[13] R. Warren, F. Sammoura, F. Tounsi, M. Sanghadasa, L. W. Lin, *J. Mater. Chem. A.* **2015**, *3*, 15568.
[14] E. Kao, C. Yang, R. Warren, A. Kozinda, L. W. Lin, *Sen. Actuators A* **2016**, *240*, 160.
[15] L. M. Suo, O. Borodin, T. Gao, M. Olguin, J. Ho, X. L. Fan, C. Luo, C. S. Wang, K. Xu, *Science* **2015**, *350*, 938.
[16] L. Smith, B. Dunn, *Science* **2015**, *350*, 918.
[17] P. Simon, Y. Gogotsi, *Nat. Mater.* **2008**, *7*, 845.

[18] M. Acerce, D. Voiry, M. Chhowalla, *Nat. Nanotechnol.* **2015**, *10*, 313.
[19] M. Ghidiu, M. R. Lukatskaya, M. Q. Zhao, Y. Gogotsi, M. W. Barsoum, *Nature* **2014**, *516*, 78.
[20] J. P. Liu, J. Jiang, C. W. Cheng, H. X. Li, J. X. Zhang, H. Gong, H. J. Fan, *Adv. Mater.* **2011**, *23*, 2076.
[21] G. H. Yu, L. B. Hu, M. Vosgueritchian, H. L. Wang, X. Xie, J. R. McDonough, X. Cui, Y. Cui, Z. N. Bao, *Nano Lett.* **2011**, *11*, 2905.
[22] Y. X. Xu, Z. Y. Lin, X. Zhong, X. Q. Huang, N. O. Weiss, Y. Huang, X. F. Duan, *Nat. Commun.* **2014**, *5*, 4554.
[23] C. C. Hu, K. H. Chang, M. C. Lin, Y. T. Wu, *Nano Lett.* **2006**, *6*, 2690.
[24] M. Toupin, T. Brousse, D. Belanger, *Chem. Mater.* **2004**, *16*, 3184.
[25] J. Musschoot, Q. Xie, D. Deduytsche, S. Van den Berghe, R. L. Van Meirhaeghe, C. Detavernier, *Microelectron. Eng.* **2009**, *86*, 72.
[26] S. W. Choi, C. M. Jang, D. Y. Kim, J. S. Ha, H. S. Park, W. Koh, C. S. Lee, *J. Korean Phys. Soc.* **2003**, *42*, S975.
[27] A. Lewandowski, A. Olejniczak, M. Galinski, I. Stepniak, *J. Power Sources* **2010**, *195*, 5814.
[28] M. Lovric, M. Hermes, F. Scholz, *J. Solid State Electrochem.* **1998**, *2*, 401.
[29] S. D. Tilley, M. Schreier, J. Azevedo, M. Stefik, M. Graetzel, *Adv. Funct. Mater.* **2014**, *24*, 303.
[30] D. H. Deng, K. S. Novoselov, Q. Fu, N. F. Zheng, Z. Q. Tian, X. H. Bao, *Nat. Nanotechnol.* **2016**, *11*, 218.
[31] Y. J. Han, X. Yue, Y. S. Jin, X. D. Huang, P. K. Shen, *J Mater. Chem A.* **2016**, *4*, 3673.
[32] V. Augustyn, P. Simon, B. Dunn, *Energy Environ. Sci.* **2014**, *7*, 1597.
[33] M. Chintapalli, K. Timachova, K. R. Olson, S. J. Mecham, D. Devaux, J. M. DeSimone, N. P. Balsara, *Macromolecules* **2016**, *49*, 3508.
[34] Y. Huang, W. S. Ip, Y. Y. Lau, J. Sun, J. Zeng, N. S. S. Yeung, W. S. Ng, H. Li, Z. Pei, Q. Xue, Y. Wang, J. Yu, H. Hu, C. Zhi, *ACS Nano* **2017**, *11*, 8953.
[35] Y. Huang, J. Tao, W. Meng, M. Zhu, Y. Huang, Y. Fu, Y. Gao, C. Zhi, *Nano Energy* **2015**, *11*, 518.
[36] Y. W. Zhu, S. Murali, M. D. Stoller, K. J. Ganesh, W. W. Cai, P. J. Ferreira, A. Pirkle, R. M. Wallace, K. A. Cychosz, M. Thommes, D. Su, E. A. Stach, R. S. Ruoff, *Science* **2011**, *332*, 1537.
[37] C. G. Liu, Z. N. Yu, D. Neff, A. Zhamu, B. Z. Jang, *Nano Lett.* **2010**, *10*, 4863.
[38] D. Sheberla, J. C. Bachman, J. S. Elias, C. J. Sun, Y. Shao-Horn, M. Dinca, *Nat. Mater.* **2017**, *16*, 220.